Supporting Information

Chestnut-like Copper Cobalt Phosphide Catalyst for All-pH Hydrogen Evolution Reaction and Alkaline Water Electrolysis

Liang Yan[a], Bing Zhang[a], Junlu Zhu[a], Shanzhi Zhao[a], Yunyong Li[a,*], Bao Zhang[b], Jianjun Jiang[b], Xiao Ji[b], Haiyan Zhang[a], and Pei Kang Shen[c]

[a] *Guangdong Provincial Key Laboratory of Functional Soft Condensed Matter, School of Materials and Energy, Guangdong University of Technology, No. 100 Waihuan Xi Road, Guangzhou Higher Education Mega Center, Guangzhou, 510006, China*

E-mail: yyli@gdut.edu.cn (Y.Y. Li).

[b] *School of Optical and Electronic Information, Huazhong university of science and technology, Wuhan, 430074, China*

[c] *Collaborative Innovation Center of Sustainable Energy Materials, Guangxi University, Nanning, Guangxi, 530004, China*

Experimental section

Chemicals. All the chemicals were directly used as received without further purification. Cobalt (II) acetate tetrahydrate ($Co(CH_3COO)_2 \cdot 4H_2O$), Copper nitrate trihydrate ($Cu(NO_3)_2 \cdot 3H_2O$), NH_4F, urea and $NaH_2PO_2 \cdot H_2O$ were purchased from Aladdin Chemical Reagent Co., Ltd. Pt/C (20% Pt on Vulcan XC-72R) and iridium oxide nanoparticles (IrO_2) were purchased from Sigma-Aldrich Chemical Reagent Co., Ltd. Nafion solution (5%) was purchased from Dupont Co., Ltd. Carbon fiber paper (TGP-H-060, thickness: 0.19 mm, electrical resistivity in through plane is 80 mΩ cm and in plane is 5.8 mΩ cm). Highly purified N_2 were supplied by Guang Zhou Sheng Ying Gas Co., Ltd. Ultrapure water (resistivity: $\rho \geq 18$ MΩ cm^{-1}) was used to prepare the solutions.

Electrodes preparation.

Synthesis of $Cu_xCo_{1-x}(OH)F/CP$ precursors and $Cu_xCo_{1-x}P/CP$ electrodes: The $Cu_xCo_{1-x}(OH)F/CP$ (x = 0, 0.025, 0.05, 0.075 and 0.1) precursors were prepared by simple hydrothermal method. In a typical synthesis, $Co(CH_3COO)_2 \cdot 4H_2O$ and $Cu(NO_3)_2 \cdot 3H_2O$ were weighed in the stoichiometric amounts, keeping the total molar mass 2 mmol. Then, $Co(CH_3COO)_2 \cdot 4H_2O$, $Cu(NO_3)_2 \cdot 3H_2O$, 4 mmol NH_4F, and 8 mmol urea were dissolved in 40 ml of distilled water, and the mixture was stirred 30 min to form a uniform solution. Then, the above solution was transferred to a 50 ml Teflon-lined stainless steel autoclave containing the CP (2 x 2.5 cm^2). Before being used, the CP was sequentially cleaned with diluted HNO_3 (1 M), ethanol and deionized water to remove the surface impurity. Subsequently, it was sealed and

maintained at 120 °C for 6 h in an electric oven. After the autoclave naturally cooled to room temperature, the $Cu_xCo_{1-x}(OH)F$/CP was taken out, washed with ethanol and water thoroughly, and dried at 60 °C for overnight.

The $Cu_xCo_{1-x}P$/CP electrodes were prepared by a low-temperature phosphidation process. To prepare $Cu_xCo_{1-x}P$/CP, $Cu_xCo_{1-x}(OH)F$/CP and $NaH_2PO_2 \cdot H_2O$ were placed at two separate positions in one porcelain crucible in the presence of $NaH_2PO_2 \cdot H_2O$ at the upstream side of the furnace. The molar ratio of Co to P was 1:10. Subsequently, the samples were heated to 300 °C with a heating rate of 3 °C min^{-1} for 2 h under N_2 atmosphere. After cooling, the loading of $Cu_xCo_{1-x}P$ on CP was determined by weighing the mass of the CP before and after catalyst growth. The mass loading of $Cu_xCo_{1-x}P$ on CP was about 5 mg cm^{-2}.

Preparation of Cu_3P/CF, Pt/C/CP and IrO_2/CP electrodes: For comparison, Cu_3P nanowire arrays on copper foam (CF) was synthesized according to reported work.[1] To prepare Pt/C/CP or IrO_2/CP electrodes, 5 mg of commercial Pt/C or IrO_2 were dispersed in 950 μL solution of ethanol, then addition of 50 μL 5 wt% Nafion solution, followed by ultrasound for at least 30 min to form a homogeneous catalyst ink. Then the catalyst ink was coated onto a CP (1 x 1 cm^2) to achieve the sample loading of 5 mg cm^{-2}.

Physical characterizations. The X-ray diffraction (XRD) measurements were performed with a D8 ADVANCE diffractometer using a Cu K_α (λ = 0.15406 nm) radiation source (Bruker Co.). X-ray photoelectron spectroscopy (XPS) measurements were carried out by Escalab 250Xi with Al K_α radiation source (Thermo Fisher

Scientific Inc.). Scanning electron microscopy (SEM) measurements were performed with a SU8220 field emission scanning electron microscopy (Hitach Co.) equipped with energy dispersive X-ray spectrometry (EDS) with an acceleration voltage of 30 kV. Transmission electron microscopy (TEM), high resolution transmission electron microscopy (HR-TEM) and element mapping analysis were conducted on Talos F200s (FEI Co.) under an accelerating voltage of 200 kV. Raman spectra were collected on a LabRAM HR Evolution Raman spectrometer with 532 nm wavelength incident laser light. Fourier transform infrared spectroscopy (FTIR) was recorded on a Nicolet IS50 spectrometer.

Electrochemical measurements. All the electrochemical measurements were performed with PGSTAT302N potentiostat/galvanostat (Metrohm Autolab, Netherlands). A conventional three-electrode glass cell was used, the synthesized $Cu_xCo_{1-x}P$/CP was directly used as the working electrode, a graphite plate was used as the counter electrode and a reversible hydrogen electrode (RHE) was used as the reference electrode. Before the HER test, all of the electrolytes (0.5 M H_2SO_4, 1.0 M KOH and 1.0 M PBS) were bubbled with high-purity N_2 for at least 30 min to remove the dissolved oxygen. For OER test, the electrolyte was saturated by O_2 for at least 30 min before the measurements. The electrodes were first cycled by 20 cyclic voltammetry (CV) scans at a scan rate of 100 mV s^{-1} until it reaches a steady state, the linear sweep voltammetry (LSV) with the scan rate of 5 mV s^{-1} was then performed. Stability tests were measured by CV scanning from 0.1 V to -0.4 V for HER (or 1.3 V to 1.8 V for OER) for 1000 cycles with the scan rate of 100 mV s^{-1}. The long-term

stability of $Cu_xCo_{1-x}P$/CP was assessed through chronopotentiometry, which was conducted with the current density holding at 10 mA cm^{-2}. All the tests were corrected for the *iR* corrections. Electrochemical impedance spectroscopy (EIS) measurements were measured at potentiostatic mode with 5 mV amplitude in a frequency range from 100 kHz to 0.01 Hz. The overall water splitting test was carried out in a two-electrode system by directly using $Cu_xCo_{1-x}P$/CP as both the cathode and anode electrode in 1.0 M KOH electrolyte.

Computational methods

The DFT calculations[2, 3] are performed by using Vienna Ab-initio Simulation Package (VASP)[4] with Projector Augmented Wave (PAW) method.[5] And the exchange-correlation energy is described by the functional of Perderw, Burke, and Ernzerhof (PBE) form.[6, 7] The kinetic energy cutoff of electron wave functions is 500 eV. The Coulomb and exchange interactions in the pristine and Cu-doped CoP (111) and β-CoOOH (012) systems were described by setting the effective on-site Coulomb and exchange parameters U-J to be 3.4 eV and 4.0 eV for Co and Cu respectively. The geometry optimizations are performed by using the conjugated gradient method, and the convergence threshold is set to be 10^{-4} eV in energy and 0.01 eV $Å^{-1}$ in force. A vacuum layer of 15 Å is applied for all calculated models.

The free energy of hydrogen adsorption at 300 K can be calculated by:

$$\Delta G_H = E_{sur-H} - 1/2E_{H_2} - E_{sur} + 0.24\ eV$$

The thermodynamic model of water oxidation proposed by Norskov and co-workers,[8] which is composed of four electrochemical steps, each of which

constitutes one proton transfer, were used in this work. The following electron reaction paths are considered for oxygen evolution reaction (OER) process:

$$H_2O(l) + * \rightleftharpoons HO* + H^+ + e^- \quad (\Delta G_1) \qquad (1)$$

$$HO* \rightleftharpoons O* + H^+ + e^- \quad (\Delta G_2) \qquad (2)$$

$$O* + H_2O(l) \rightleftharpoons HOO* + H^+ + e^- \quad (\Delta G_3) \qquad (3)$$

$$HOO* \rightleftharpoons O_2(g) + * + H^+ + e^- \quad (\Delta G_4) \qquad (4)$$

where * represents an active site on the γ-Al_2O_3 surface. O*, OH* and OOH* are intermediates adsorbed on the active site. ΔG_{1-4} are the Gibbs free energies change for the above four elementary steps. Zero point energy (ZPE) corrections and thermal enthalpy and entropy contributions (TS) to the free energies are retrieved from literature.[9]

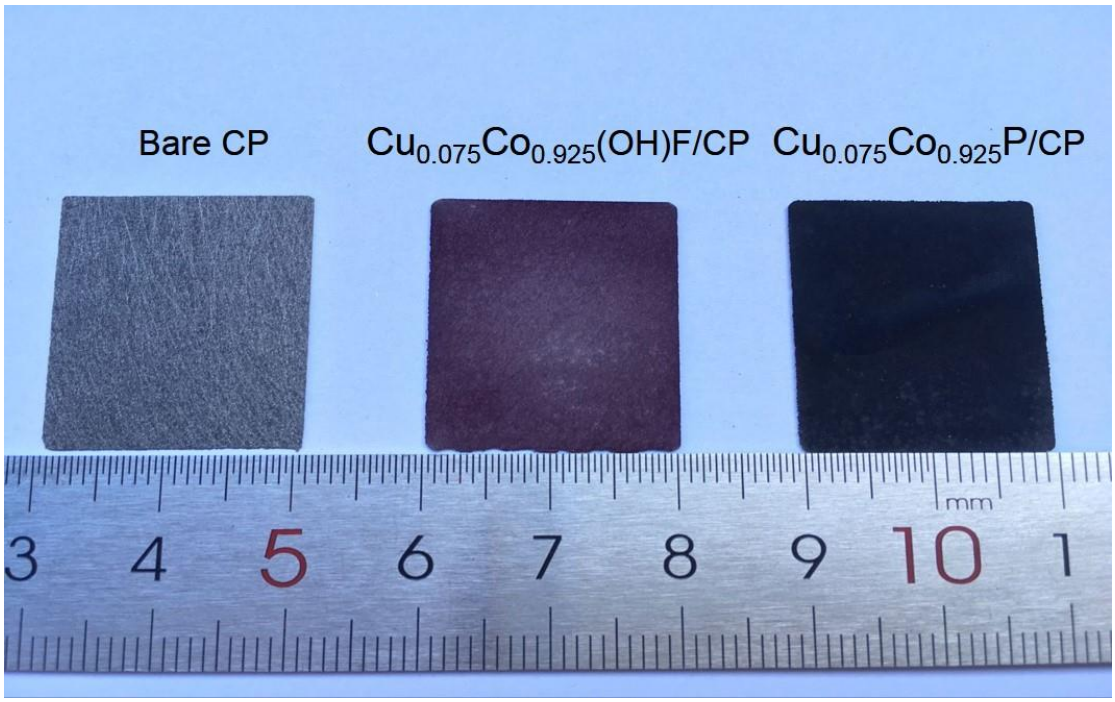

Figure S1. Optical photographs of bare CP, $Cu_{0.075}Co_{0.925}(OH)F$/CP, and $Cu_{0.075}Co_{0.925}P$ /CP.

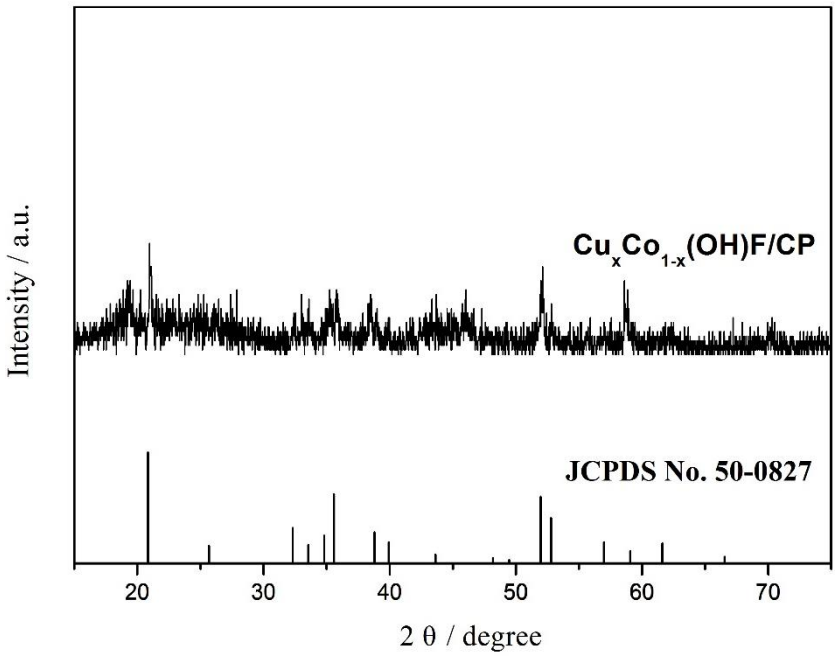

Figure S2. XRD pattern of as-prepared $Cu_xCo_{1-x}(OH)F/CP$.

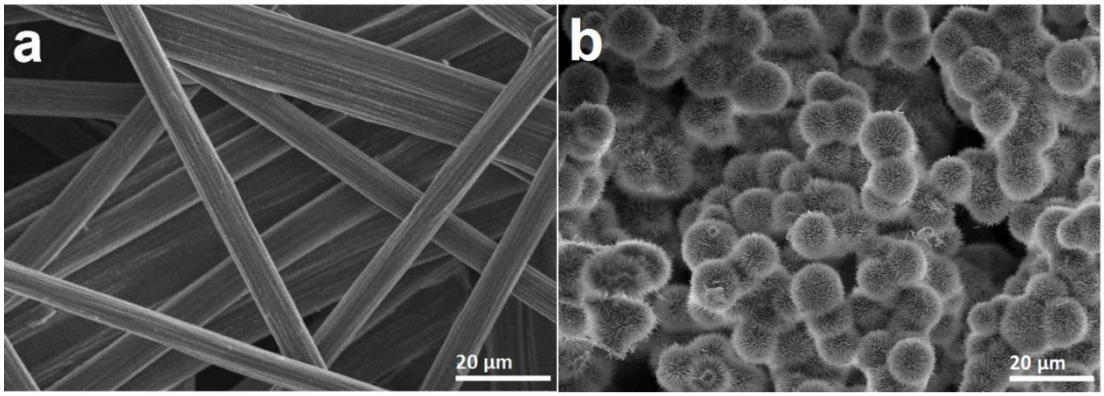

Figure S3. SEM images of (a) bare CP and (b) $Cu_{0.075}Co_{0.925}P/CP$.

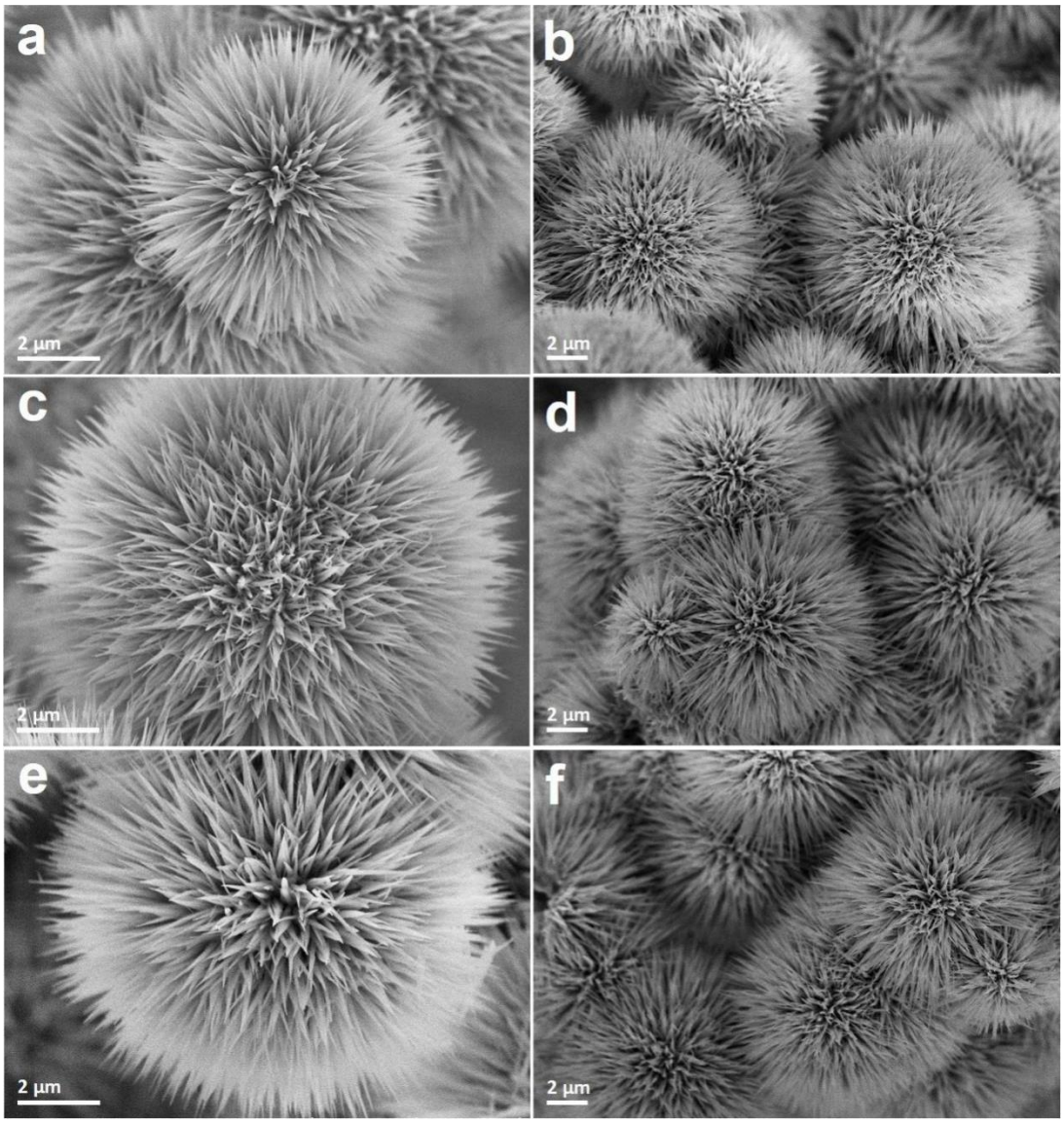

Figure S4. SEM images of (a) $Cu_{0.025}Co_{0.975}(OH)F/CP$, (c) $Cu_{0.05}Co_{0.95}(OH)F/CP$, (e) $Cu_{0.1}Co_{0.9}(OH)F/CP$ and after the phosphidation of (b) $Cu_{0.025}Co_{0.975}P/CP$, (d) $Cu_{0.05}Co_{0.95}P/CP$, (f) $Cu_{0.1}Co_{0.9}P/CP$.

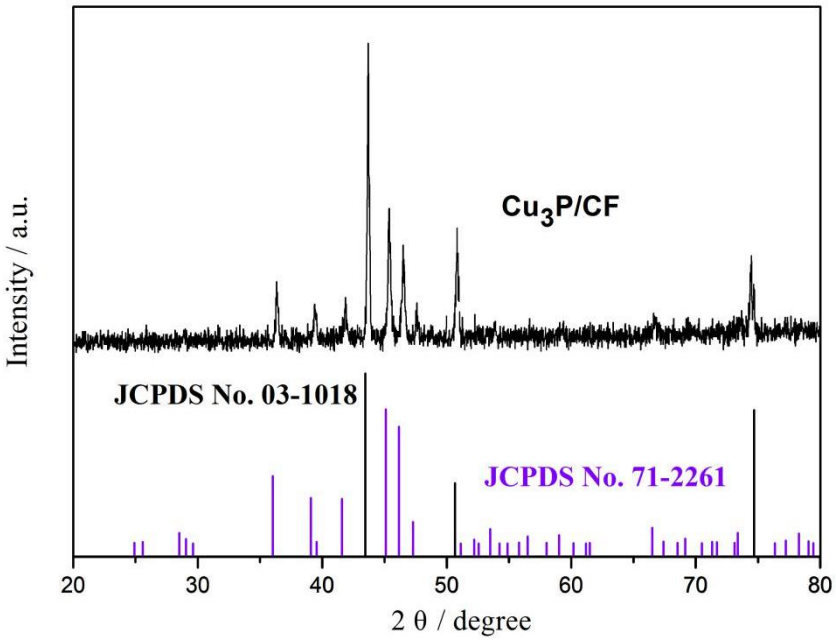

Figure S5. XRD pattern of as-prepared Cu_3P/CF.

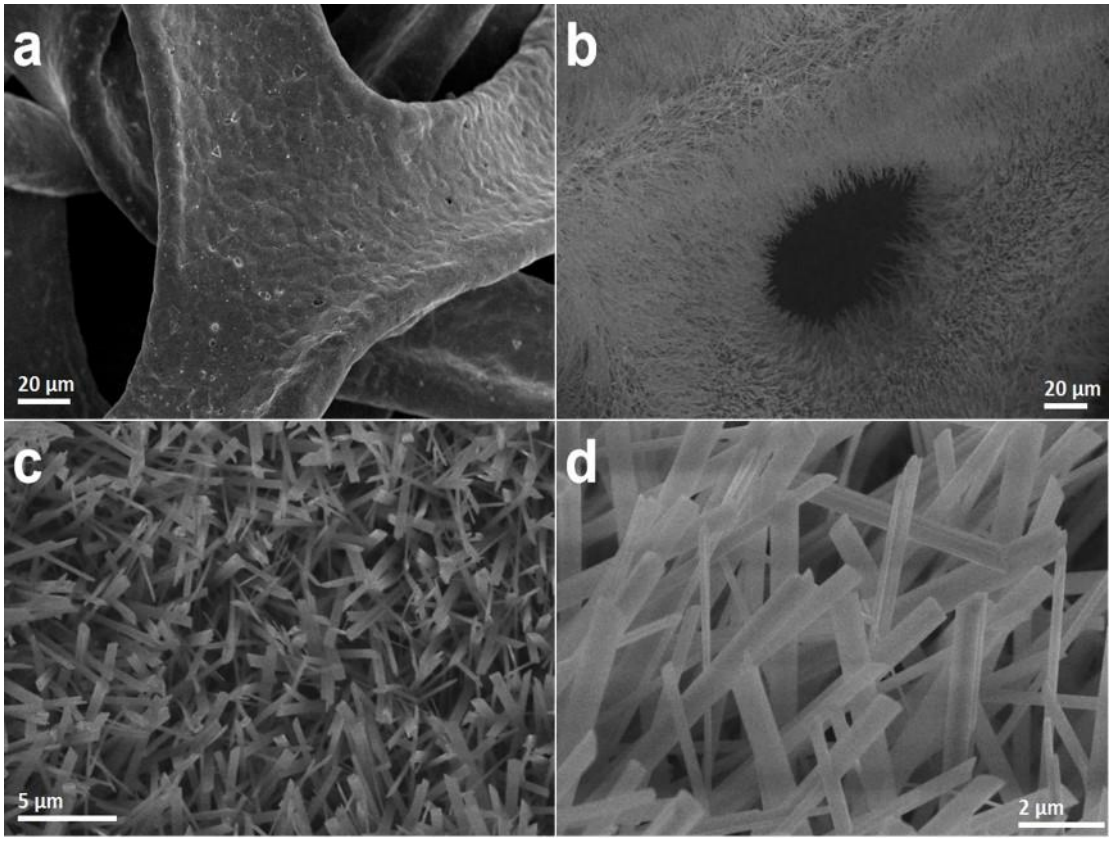

Figure S6. SEM images of (a) bare CF and (b-d) Cu_3P/CF at varied magnifications.

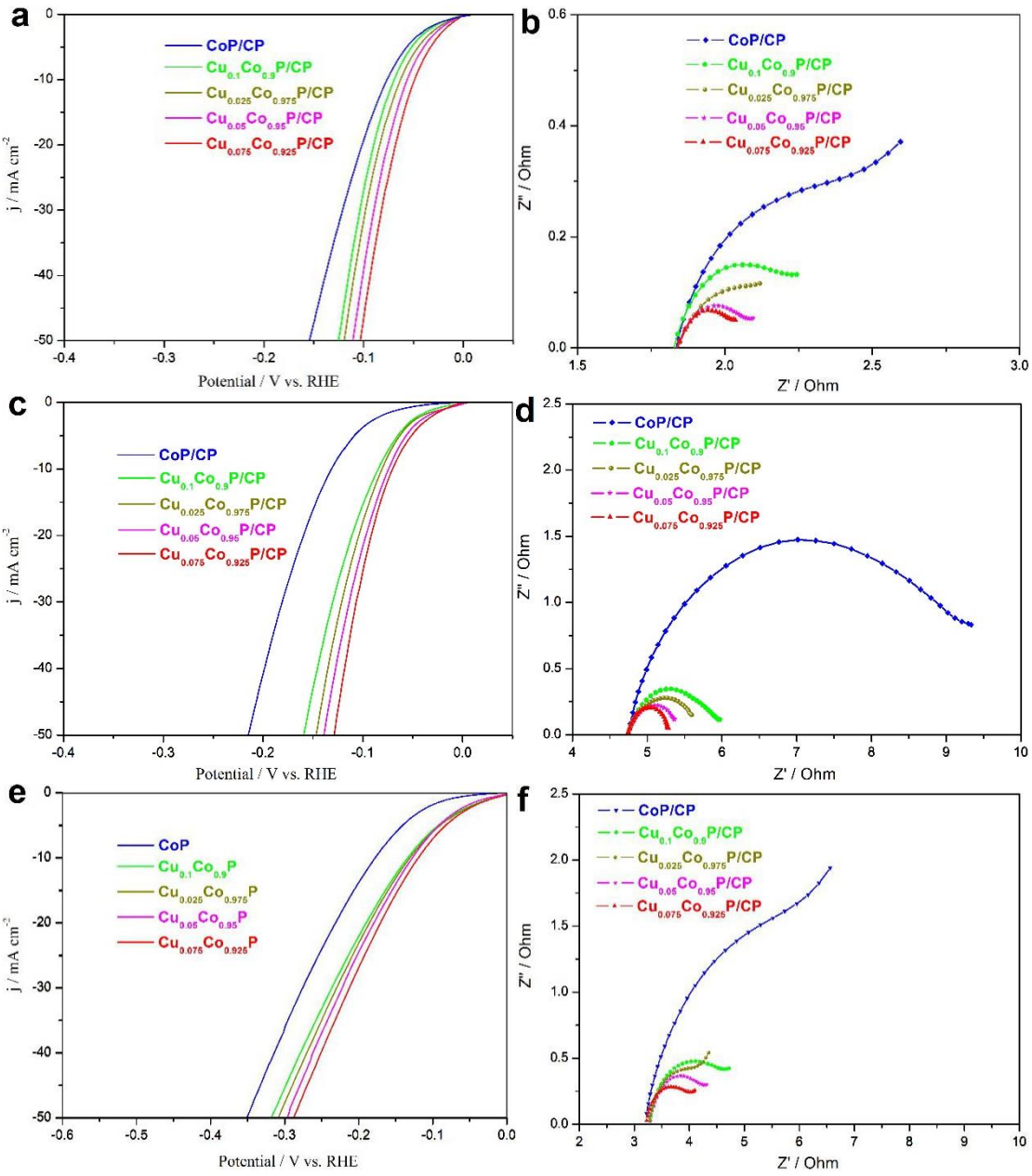

Figure S7. HER performances of the $Cu_xCo_{1-x}P/CP$ (x = 0, 0.025, 0.05, 0.075, and 0.1) in (a) 0.5 M H_2SO_4 (c) 1.0 M KOH, and (e) 1.0 M PBS, respectively. EIS Nyquist plots of the $Cu_xCo_{1-x}P/CP$ (x = 0, 0.025, 0.05, 0.075, and 0.1) in (b) 0.5 M H_2SO_4, (d) 1.0 M KOH, and (f) 1.0 M PBS, respectively.

Electrochemical active surface area (ECSA): The ECSA of different samples was estimated from the double-layer capacitance (C_{dl}), which can be measured using a simple CV method with ten different scan rates (10-100 mV/s) in non-faradaic potential region.[10] In this potential region, all measured currents are assumed to be associated with double-layer charging, which is expected to be linearly proportional to the ECSA. By plotting the capacitive currents $j = (j_{anodic}-j_{cathodic})/2$ against the scan rates, and following with a linear fit, the C_{dl} can be determined from the slope. The C_{dl} can be further converted into ECSA using the specific capacitance value for a standard with 1 cm^2 of real surface area. The ECSA of different samples can be calculated according to the following equation:

$$A_{ECSA}^{Catalysts} = \frac{C_{dl}\text{-catalysts (mF cm}^{-2})}{C_{dl}\text{ - standard (mF cm}^{-2}) \text{ per cm}^2_{ECSA}}$$

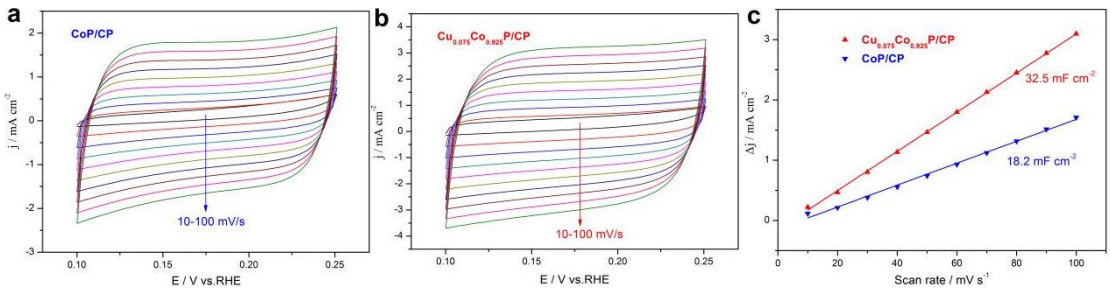

Figure S8. CVs for CoP /CP (a) and $Cu_{0.075}Co_{0.925}P$/CP (b) at different scan rates in 0.5 M H_2SO_4. (c) Linear fitting curves of the capacitive currents as a function of scan rates for CoP /CP and $Cu_{0.075}Co_{0.925}P$/CP.

Turnover frequency (TOF): To calculate TOF, Cyclic voltammetry measurements was performed in 1.0 M PBS (pH=7) within the potential range of -0.2 to 0.6 V (vs. RHE) at a scan rate of 50 mV s^{-1}.[11] When the number of active sites (n) was determined, the TOF was calculated with the equation:

$$TOF = I/2nF$$

Where I represent the current (A) during the LSV measurement in 0.5 M H_2SO_4, F is the Faraday constant (96485 $C \cdot mol^{-1}$), and n is the number of active sites (mol). In the equation, 1/2 represents that two protons to form one hydrogen molecule need two electrons.

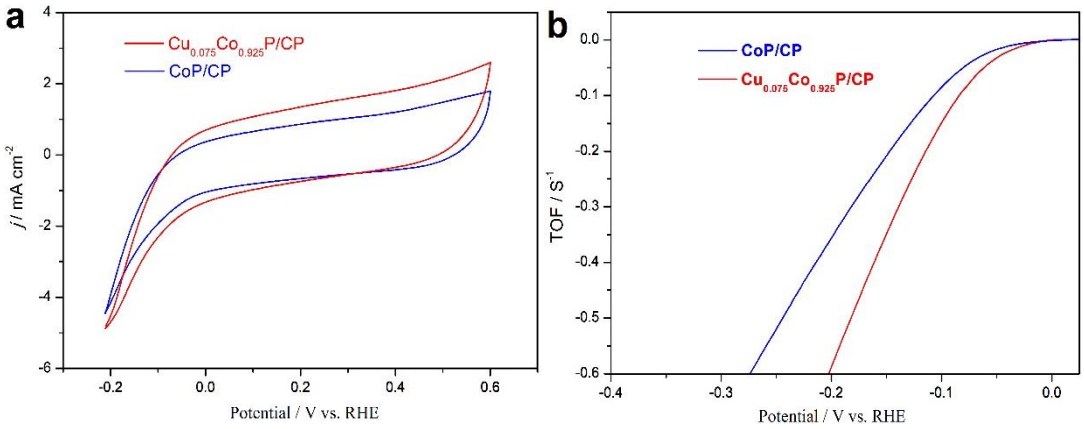

Figure S9. (a) CV curves of CoP/CP and $Cu_{0.075}Co_{0.925}P$ /CP in 1.0 M PBS at a scan rate of 50 mV/s. (b) Calculated TOF of CoP/CP and $Cu_{0.075}Co_{0.925}P$ /CP in 0.5 M H_2SO_4.

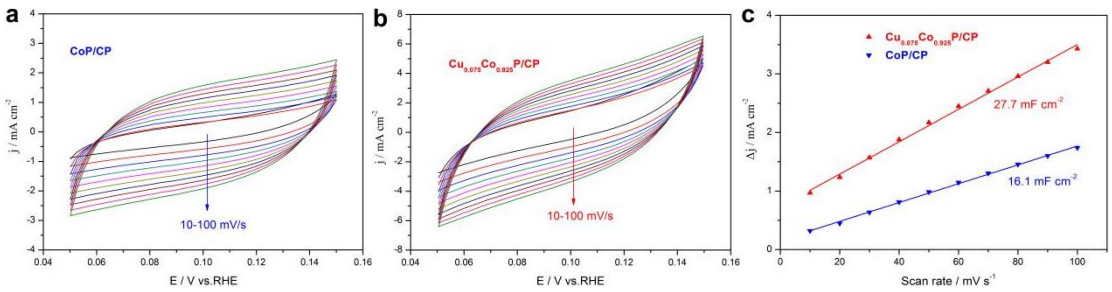

Figure S10. CVs for CoP /CP (a) and $Cu_{0.075}Co_{0.925}P$/CP (b) at different scan rates in 1.0 M KOH. (c) Linear fitting curves of the capacitive currents as a function of scan rates for CoP /CP and $Cu_{0.075}Co_{0.925}P$/CP.

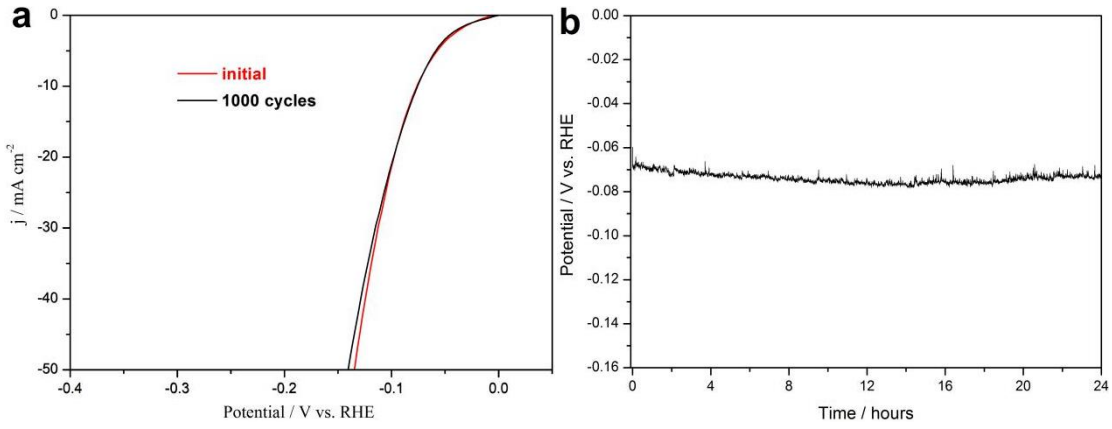

Figure S11. Continuous CV curves (a) and chronopotentiometry at 10 mA cm^{-2} (b) of $Cu_{0.075}Co_{0.0925}P$/CP in 1.0 M KOH.

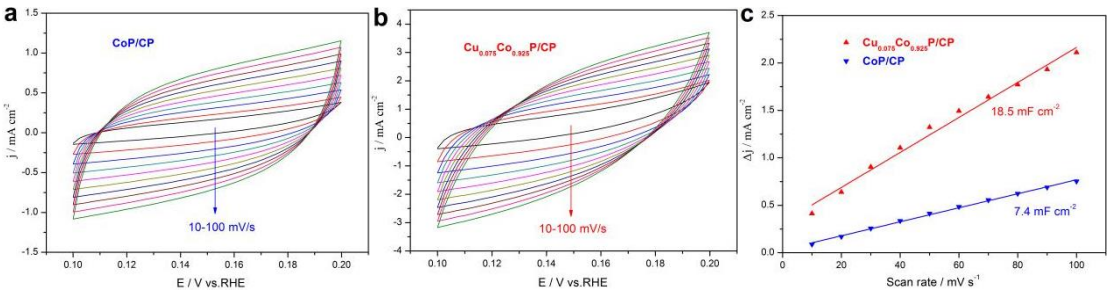

Figure S12. CVs for CoP /CP (a) and $Cu_{0.075}Co_{0.925}P$/CP (b) at different scan rates in 1.0 M PBS. (c) Linear fitting curves of the capacitive currents as a function of scan rates for CoP /CP and $Cu_{0.075}Co_{0.925}P$/CP.

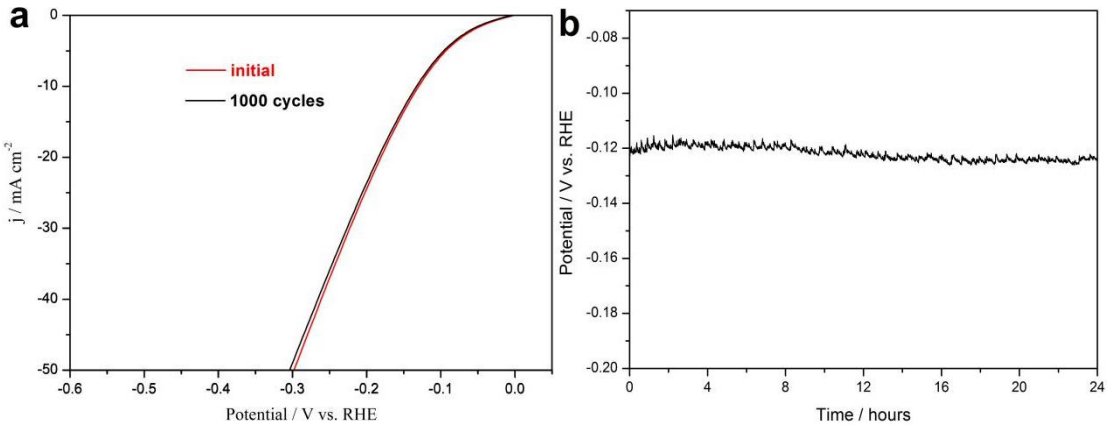

Figure S13. Continuous CV curves (a) and chronopotentiometry at 10 mA cm^{-2} (b) of $Cu_{0.075}Co_{0.0925}P$/CP in 1.0 M PBS.

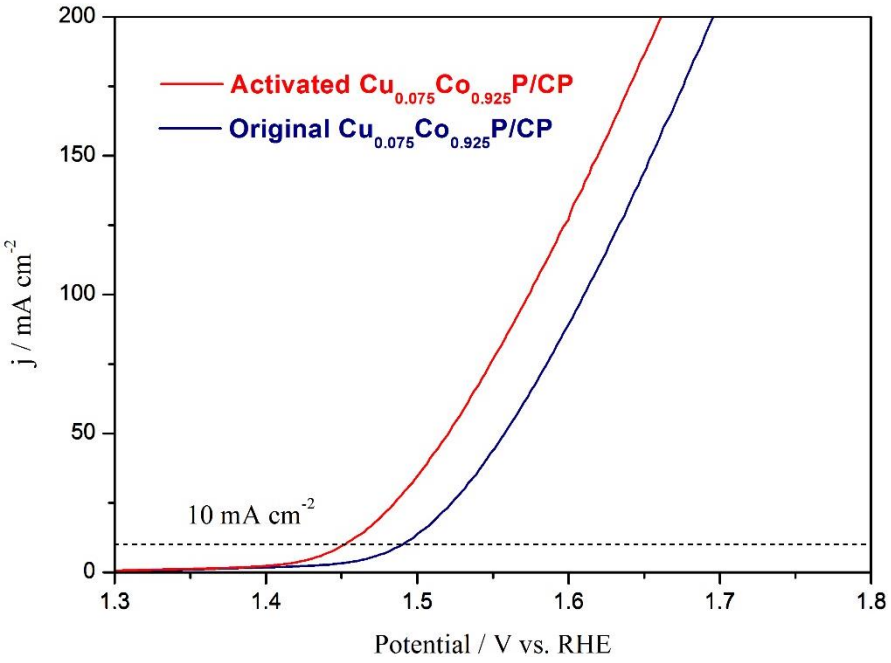

Figure S14. OER performances of the $Cu_{0.075}Co_{0.0925}P$/CP before and after activation.

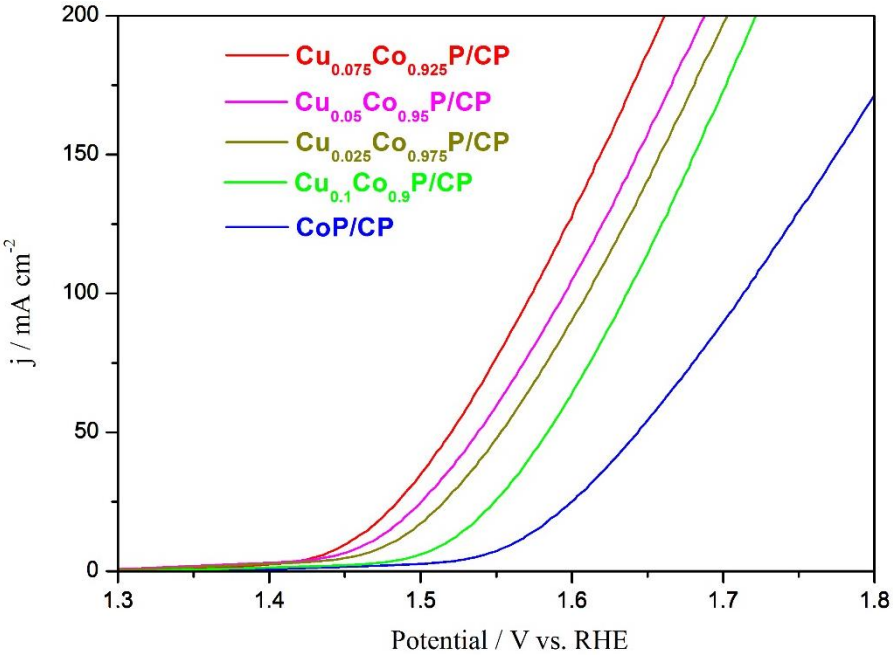

Figure S15. OER performances of the $Cu_xCo_{1-x}P$/CP (x = 0, 0.025, 0.05, 0.075, and 0.1) in 1.0 M KOH.

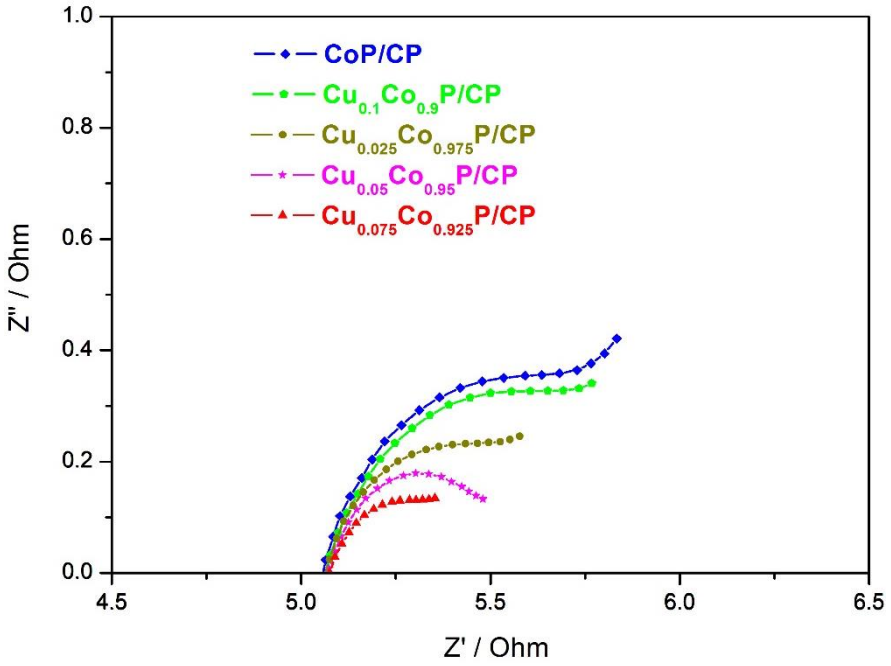

Figure S16. EIS Nyquist plots of the $Cu_xCo_{1-x}P/CP$ (x = 0, 0.025, 0.05, 0.075, and 0.1) at overpotential of 250 mV in 1.0 M KOH for OER.

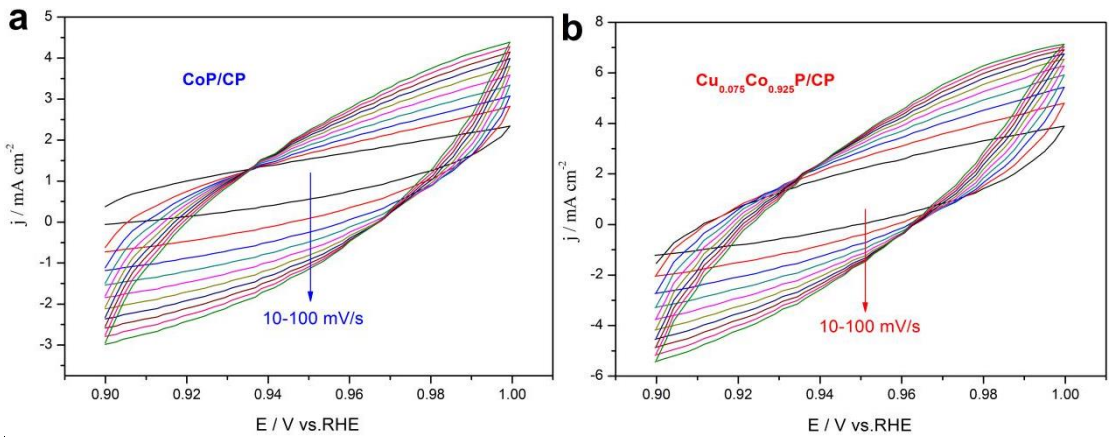

Figure S17. CVs for (a) CoP /CP and (b) $Cu_{0.075}Co_{0.925}P/CP$ at different scan rates in 1.0 M KOH for OER.

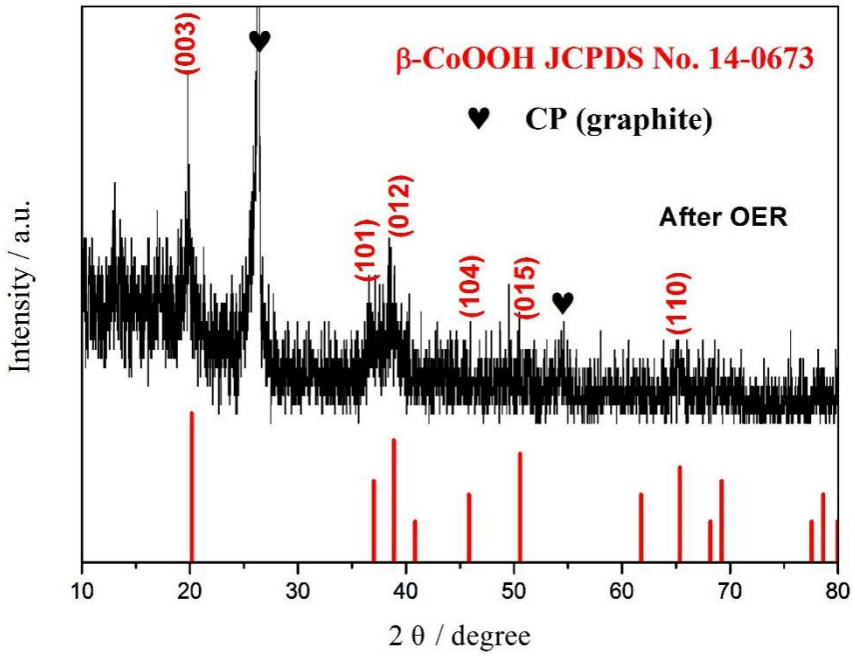

Figure S18. XRD pattern of the $Cu_{0.075}Co_{0.925}P$/CP after OER electrolysis.

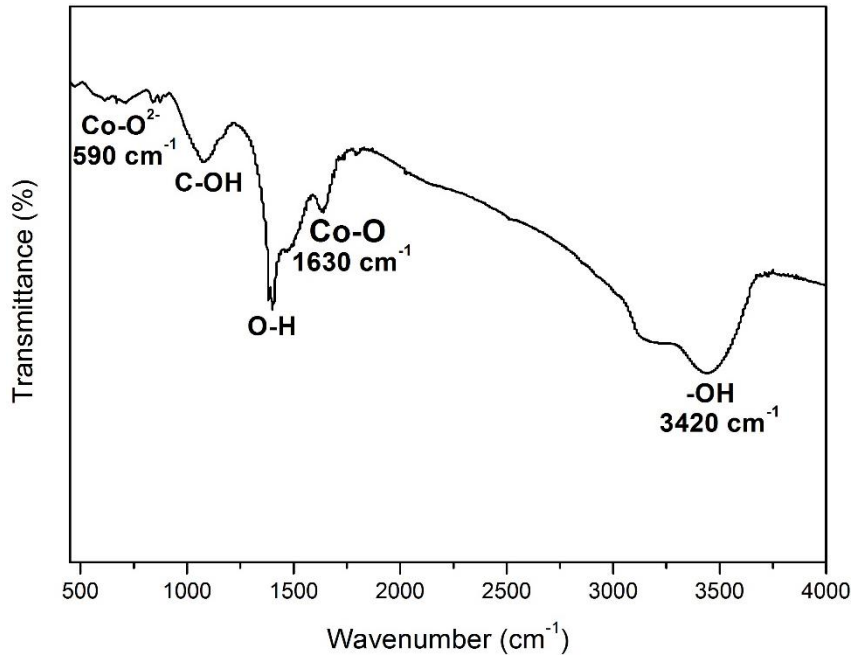

Figure S19. FTIR spectrum of the $Cu_{0.075}Co_{0.925}P$/CP after OER electrolysis.

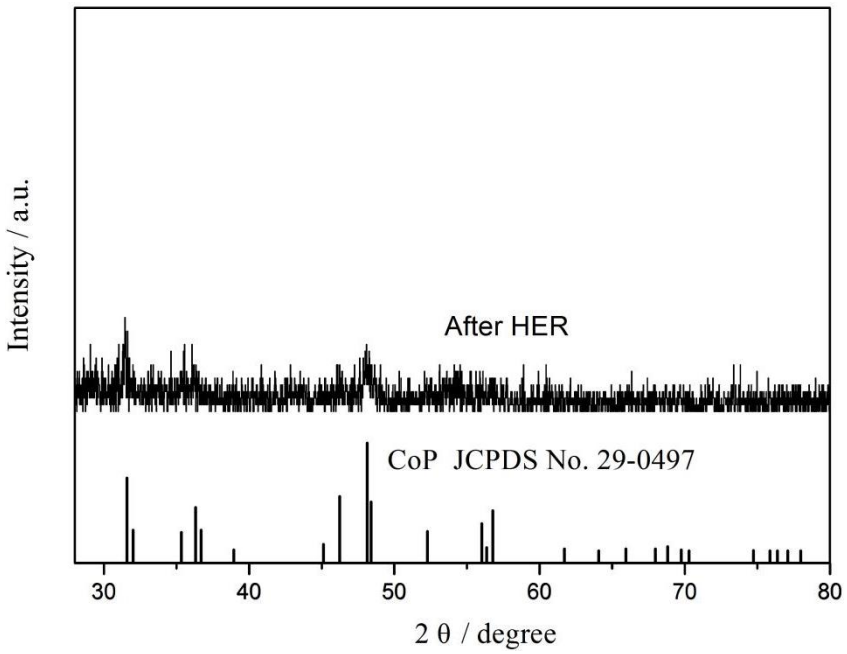

Figure S20. XRD pattern of the $Cu_{0.075}Co_{0.925}P$/CP after HER electrolysis.

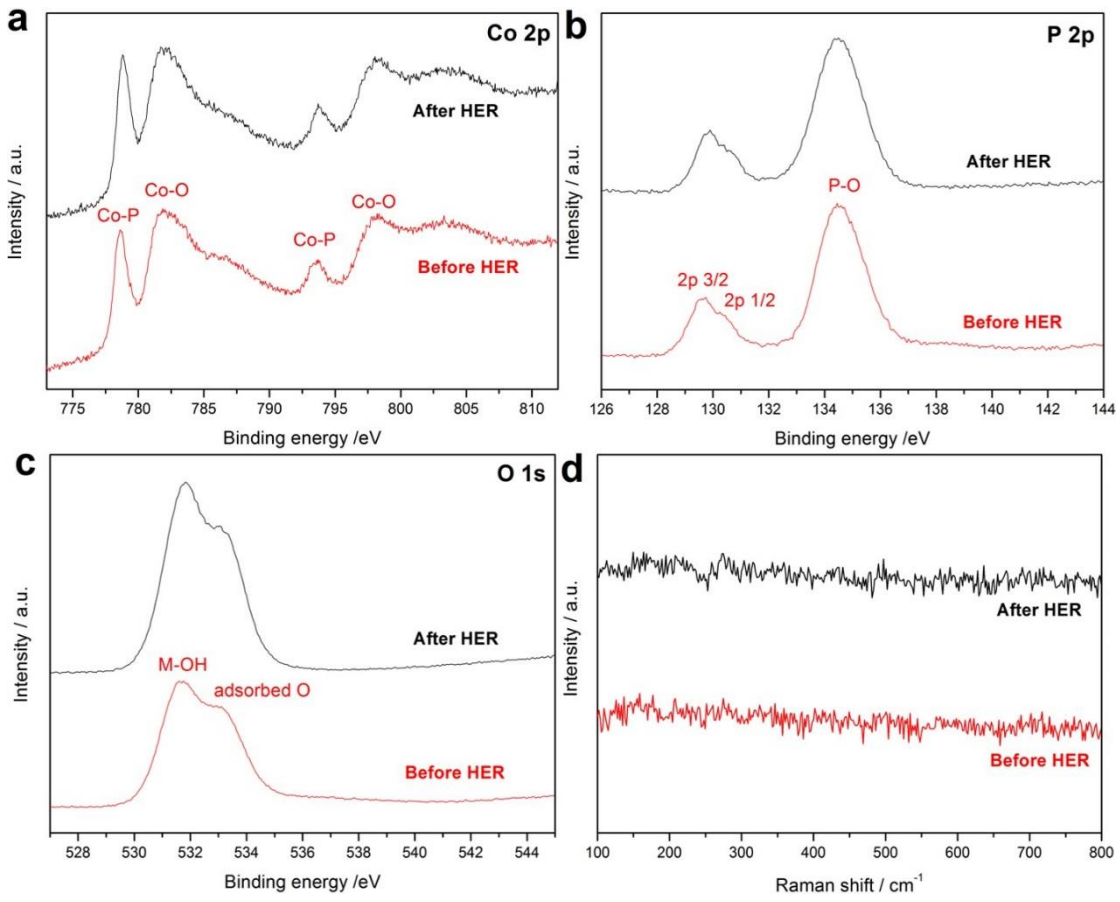

Figure S21 High-resolution XPS spectra of $Cu_{0.075}Co_{0.0925}P$/CP for (a) Co 2p, (b) P 2p, (c) O 1s, and (d) Raman spectra before and after HER tests.

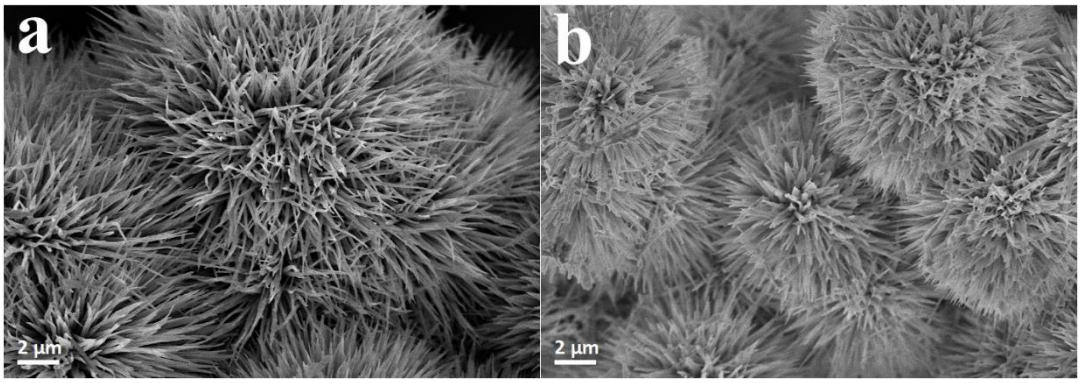

Figure S22. SEM images of the $Cu_{0.075}Co_{0.0925}P$/CP after (a) HER and (b) OER test.

Table S1. HER performance of the $Cu_{0.075}Co_{0.0925}P$/CP in this work, in comparison with other non-noble metal based catalysts in 0.5 M H_2SO_4 from recent publications. (η: overpotential)

Catalysts	η (mV) at 10 mA cm^{-2}	Tafel slope mV dec^{-1}	Reference
CoP/CC	67	51	J. Am. Chem. Soc. **2014**, *136*, 7587.
CoP/CNT	122	54	Angew. Chem. Int. Ed. **2014**, *53*, 6710.
CoP/Ti	~75	50	Angew. Chem. Int. Ed. **2014**, *53*, 5427.
CoPS NWs	61	48	Nat. Mater. **2015**, *14*, 1245.
Co_2P NPs	95	45	Chem. Mater. **2015**, *27*, 3769.
CoNiP@NF	60	39	J. Mater. Chem. A **2016**, *4*, 10195.
np-$(Co_{0.52}Fe_{0.48})_2P$	64	45	Energy Environ. Sci. **2016**, *9*, 2257.
$Ni_{0.62}Co_{0.38}P$	166	72	Adv. Funct. Mater. **2016**, *26*, 7644.
$NiCo_2P_x$/CF	104	59.6	Adv. Mater. **2017**, *29*, 1605502.
Mn-Co-P/Ti	49	55	ACS Catal. **2017**, *7*, 98.
Ce-CoP NWs/Ti	54	54	Nano Energy **2017**, *38*, 290.
CoP@BCN-1	87	46	Adv. Energy Mater. **2017**, *7*, 1601671.
CoP/NCNHP	140	53	J. Am. Chem. Soc. **2018**, *140*, 2610.
PANI/CoP HNWs-CFs	57	34.5	J. Am. Chem. Soc. **2018**, *140*, 5118.
Ni-CoP/HPFs	144	52	Nano Energy **2019**, *56*, 411.
Co-P@PC-750	72	49	Small **2019**, 1900550.
Er-doped CoP	52	32	J. Mater. Chem. A **2019**, *7*, 5769.
N-Co_2P/CC	27	45	ACS Catal. **2019**, *9*, 3744.
CoP/Co-MOF	27	43	Angew. Chem. Int. Ed. **2019**, *58*, 4679.
CoP/NiCoP/NC	60	58	Adv. Funct. Mater. **2019**, *29*, 1807976.
$Cu_{0.075}Co_{0.0925}P$/CP	47	47.2	This work

Table S2. HER performance of the $Cu_{0.075}Co_{0.0925}P$/CP in this work, in comparison with other non-noble metal based catalysts in 1.0 M KOH from recent publications.

Catalysts	η (mV) at 10 mA cm^{-2}	Tafel slope mV dec^{-1}	Reference
CoP/CC	209	129	J. Am. Chem. Soc. **2014**, *136*, 7587.
Co-P film	94	42	Angew. Chem. Int. Ed. **2015**,*54*,6251.
CoP NS/C	111	70.9	Green Chem. **2016**, *18*, 2287.
CoNiP@NF	155	113	J. Mater. Chem. A **2016**, *4*, 10195.
np-$(Co_{0.52}Fe_{0.48})_2P$	79	40	Energy Environ. Sci. **2016**, *9*, 2257.
$Ni_{0.51}Co_{0.49}P$ film	82	43	Adv. Funct. Mater. **2016**, *26*, 7644.
CoP@NC	129	58	ACS Catal. **2017**, *7*, 3824.
Mn-Co-P/Ti	76	52	ACS Catal. **2017**, *7*, 98.
Ce-CoP NWs/Ti	92	63.5	Nano Energy **2017**, *38*, 290.
Fe-CoP/Ti	78	75	Adv. Mater. **2017**, *29*, 1602441.
CoMoP@C	81	55.5	Energy Environ. Sci. **2017**, *10*, 788.
Ni-Co-P HNBs	107	46	Energy Environ. Sci. **2018**, *11*, 872.
$Co_{0.93}Ni_{0.07}P_3$/CC	87	60.7	ACS Energy Lett. **2018**, *3*, 1744.
CoP/NCNHP	115	66	J. Am. Chem. Soc. **2018**, *140*, 2610.
CoP@3D MXene	168	58	ACS Nano **2018**, *12*, 8017.
Ni-CoP/HPFs	92	71	Nano Energy **2019**, *56*, 411.
Co-P@PC-750	76	52	Small **2019**, 1900550.
Er-doped CoP	66	61	J. Mater. Chem. A **2019**, *7*, 5769.
N-Co_2P/CC	34	51	ACS Catal. **2019**, *9*, 3744.
CoP/Co-MOF	34	56	Angew. Chem. Int. Ed. **2019**,*58*,4679.
CoP/NiCoP/NC	75	64	Adv. Funct. Mater. **2019**, *29*,1807976.
$Cu_{0.075}Co_{0.0925}P$/CP	70	55.1	This work

Table S3. HER performance of the $Cu_{0.075}Co_{0.0925}P$/CP in this work, in comparison with other non-noble metal based catalysts in 1.0 M PBS from recent publications.

Catalysts	η (mV) at 10 mA cm^{-2}	Tafel slope mV dec^{-1}	Reference
CoP/CC	106	93	J. Am. Chem. Soc. **2014**, *136*, 7587.
CoP/Ti	149	111	Chem. Mater. **2014**, *26*, 4326.
$CoNi_4P_2$	430	NA	Energy Environ. Sci. **2014**, *7*, 329.
CoP-MNA/NF	~180*	189	Adv. Funct. Mater. **2015**, *25*, 7337.
NiCoP/rGO	124	91	Adv. Funct. Mater **2016**, *26*, 6785.
CoP NW/Hb	121	106	Nano Research **2017**, *10*, 1010.
Mn-Co-P/Ti	86	82	ACS Catal. **2017**, *7*, 98.
CoP@BCN-1	122	59	Adv. Energy Mater. **2017**, *7*, 1601671.
PdP_2@CB	84.6	72.3	Angew. Chem. Int. Ed. **2018**, *57*, 1.
Ni_2P@NPCNFs	185.3	230.3	Angew. Chem. Int. Ed. **2018**, *57*, 1963.
$Ni_{0.1}Co_{0.9}P$/CFP	125	103	Angew. Chem. Int. Ed. **2018**, *57*, 15445.
CoP@NPMG	126	62	Nanoscale, **2018**, *10*, 2603.
Co-P@PC-750	85	58	Small **2019**, 1900550.
np-$Co_9S_4P_4$	87	52	ACS Appl. Mater. Interfaces **2019**, *11*, 3880
N-Co_2P/CC	42	68	ACS Catal. **2019**, *9*, 3744.
CoP/Co-MOF	49	63	Angew. Chem. Int. Ed. **2019**, *58*, 4679.
CoP/NiCoP/NC	123	78	Adv. Funct. Mater. **2019**, *29*, 1807976.
$Cu_{0.075}Co_{0.0925}P$/CP	120	97.5	This work

*: In 0.5 M PBS.

Table S4. OER performance of the $Cu_{0.075}Co_{0.0925}P$/CP in this work, in comparison with other non-noble metal based catalysts in 1.0 M KOH from recent publications.

Catalysts	η (mV) at 10 mA cm^{-2}	Tafel slope mV dec^{-1}	Reference
CoP-MNA/NF	290	65	Adv. Funct. Mater. **2015**, *25*, 7337.
Co-P film	345	47	Angew. Chem. Int. Ed. **2015**, *54*, 6251.
CoP NR/C	320	71	ACS Catal. **2015**, *5*, 6874.
np-$(Co_{0.52}Fe_{0.48})_2P$	270	30	Energy Environ. Sci. **2016**, *9*, 2257.
NiCoP/NF	280	87	Nano Lett. **2016**, *16*, 7718.
CoMnP nanoparticles	330	61	J. Am. Chem. Soc. **2016**, *138*, 4006.
CoP/rGO	340	66	Chem. Sci. **2016**, *7*, 1690.
CoP NS/C	277	85.6	Green Chem. **2016**, *18*, 2287.
NiCoP/Ti	310	52	Adv. Mater. Interfaces **2016**, *3*, 1500454.
NiCoP/C	330	96	Angew. Chem. Int. Ed. **2017**, *56*, 3897.
Fe-CoP/Ti	230	67	Adv. Mater. **2017**, *29*, 1602441.
Ni-Co-P HNBs	270	76	Energy Environ. Sci. **2018**,*11*, 872.
Mo-CoOOH/CC	305	56	Nano Energy **2018**, *48*, 73.
S:CoP@NG	260	108	Nano Energy **2018**, *53*, 286.
CoP/NCNHP	310	70	J. Am. Chem. Soc. **2018**, *140*, 2610.
CoP@3D MXene	290	51	ACS Nano **2018**, *12*, 8017.
S:Co_2P@CC	290	82	Chem. Mater. **2018**, *30*, 8861
CoP@NPMG	276	54	Nanoscale, **2018**, *10*, 2603.
Co-P@PC-750	283	53	Small **2019**, 1900550
Er-doped CoP	256	70	J. Mater. Chem. A **2019**, *7*, 5769
Cr-FeNiP/NCN	240	72.36	Adv. Mater. **2019**, 1900178
$Cu_{0.075}Co_{0.0925}P$/CP	221	70.4	This work

Table S5. Summary of recent reported representative of bifunctional non-noble metal based catalysts for overall water-splitting in 1.0 M KOH.

Catalysts	Potential (V) at 10 mA cm^{-2}	Reference
Co-P film	1.65	Angew. Chem. Int. Ed. **2015**, *54*, 6251.
CoP-MNA	1.62	Adv. Funct. Mater. **2015**, *25*, 7337.
CoP NR	1.587	ACS Catal. **2015**, *5*, 6874.
np-$(Co_{0.52}Fe_{0.48})_2P$	1.53	Energy Environ. Sci. **2016**, *9*, 2257.
NiCoP/Ti	1.64	Adv. Mater. Interfaces **2016**, *3*, 1500454.
CoP/GO	1.7	Chem. Sci. **2016**, *7*, 1690.
NiCoP/NF	1.58	Nano Lett. **2016**, *16*, 7718.
Fe-CoP/Ti	1.60	Adv. Mater. **2017**, *29*, 1602441.
Co4Ni1P NTs	1.59	Adv. Funct. Mater. **2017**, *27*, 1703455.
Ni-Co-P HNBs	1.62	Energy Environ. Sci. **2018**, *11*, 872.
Mo-CoP/CC	1.56	Nano Energy **2018**, *48*, 73.
S:CoP@NF	1.617	Nano Energy **2018**, *53*, 286.
CoP/NCNHP	1.64	J. Am. Chem. Soc. **2018**, *140*, 2610.
CoP@NPMG	1.58	Nanoscale, **2018**, *10*, 2603.
CoP@3D MXene	1.58	ACS Nano **2018**, *12*, 8017.
Co-P@PC-750	1.60	Small **2019**, 1900550.
Er-doped CoP	1.58	J. Mater. Chem. A **2019**, *7*, 5769.
Cr-FeNiP/NCN	1.5	Adv. Mater. **2019**, 1900178.
$Cu_{0.075}Co_{0.0925}P$/CP	1.55	This work

References

1 J. Tian, Q. Liu, N. Cheng, A. M. Asiri and X. Sun, *Angew. Chem. Int. Ed.*, 2014, **53**, 9577-9581.

2 P. Hohenberg and W. Kohn, *Phys. Rev.* , 1964, **136**, B864-B871.

3 W. Kohn and L. J. Sham, *Phys. Rev.*, 1965, **140**, A1133-A1138.

4 G. Kresse and J. Hafner, *Phys. Rev. B*, 1993, **47**, 558-561.

5 P. E. Blöchl, *Phys. Rev. B*, 1994, **50**, 17953-17979.

6 G. Kresse and J. Furthmüller, *Phys. Rev. B*, 1996, **54**, 11169-11186.

7 J. P. Perdew, K. Burke and M. Ernzerhof, *Phys. Rev. Lett.*, 1996, **77**, 3865-3868.

8 I. C. Man, H.-Y. Su, F. Calle-Vallejo, H. A. Hansen, J. I. Martínez, N. G. Inoglu, J. Kitchin, T. F. Jaramillo, J. K. Nørskov and J. Rossmeisl, *ChemCatChem*, 2011, **3**, 1159-1165.

9 M. García-Mota, M. Bajdich, V. Viswanathan, A. Vojvodic, A. T. Bell and J. K. Nørskov, *J. Phys. Chem. C*, 2012, **116**, 21077-21082.

10 C. C. L. McCrory, S. Jung, I. M. Ferrer, S. M. Chatman, J. C. Peters and T. F. Jaramillo, *J. Am. Chem. Soc.*, 2015, **137**, 4347-4357.

11 Y. Pan, K. Sun, Y. Lin, X. Cao, Y. Cheng, S. Liu, L. Zeng, W.-C. Cheong, D. Zhao, K. Wu, Z. Liu, Y. Liu, D. Wang, Q. Peng, C. Chen and Y. Li, *Nano Energy*, 2019, **56**, 411-419.